Article

Single-cell transcriptome analysis identifies MIF as a novel tumor-associated neutrophil marker for pancreatic ductal adenocarcinoma

Check for updates

Yan Zeng[1,3], Jiaping Yu[1,3], Yutong Chen[1,2,3], Juan Zhuang[1], Xinyue Liang[1], Yaning Li[1], Shili Chen[1] ✉, Wenzheng Pang[1] ✉ & Linjuan Zeng[1] ✉

Pancreatic cancer is a common cause of cancer mortality, and pancreatic ductal adenocarcinoma (PDAC) is the most common subtype. Tumor-associated neutrophils (TANs) have been recognized as potential therapeutic targets. In this study, we utilized bulk and single-cell RNA sequencing (scRNA–seq) to identify seven distinct subtypes of neutrophils in PDAC. Oxidized low-density lipoprotein receptor 1 (OLR1)+ neutrophils and macrophage migration inhibitory factor (MIF)+ neutrophils were classified as TANs. The clinical relevance, dynamic transitional process, function, cell–cell communication and transcription factor activity of neutrophil subclusters in PDAC were characterized. Furthermore, the novel MIF+ TANs were fully validated in PDAC tissues, an orthotopic pancreatic tumor model and a patient-derived xenograft (PDX) model. MIF+ TANs promote the proliferation and migration of PDAC cells through the activation of the ERK and AKT pathways and epithelial–mesenchymal transition (EMT). This study provides insight into the potential of MIF+ TANs as therapeutic targets for PDAC patients.

Pancreatic cancer, which mainly consists of pancreatic ductal adenocarcinoma (PDAC), is a major cause of cancer-related mortality[1–3]. The 5-year survival rate of patients with pancreatic cancer approached 10% in 2020, an increase from 5.26% in 2000[1]. Despite these modest improvements, the current cytotoxic therapies for advanced PDAC have limited efficacy[4,5]. Immunotherapeutic strategies also have low efficacy PDAC treatment because of the high stromal density, which impedes T-cell infiltration[5,6]. It is necessary to activate the innate immune system in non-T-cell-infiltrated tumors, which can facilitate T-cell trafficking and facilitate adaptive immunity[7]. Therapeutic strategies aimed at the innate immune system may be alternatives to existing immunotherapies in patients with PDAC. Neutrophils contribute to antitumor responses by directly eliminating tumor cells and engaging in antitumor resistance. Conversely, tumor-associated neutrophils (TANs), which constitute a significant component of the tumor microenvironment (TME), can also contribute to tumor progression by driving angiogenesis, metastasis and immunosuppression[8–10]. It has been reported that neutrophils participate in both the initiation and progression of PDAC. Neutrophils can regulate T-cell immunosurveillance and reduce the efficacy of cytotoxic chemotherapy in patients with PDAC[11]. Bianchi et al. reported that neutrophil-derived TNF-α could maintain immunosuppression and stromal inflammation in PDAC microenvironments[12]. When combined with chemotherapy, disrupting neutrophil infiltration or inhibiting Gas6/AXL signaling can suppress metastatic pancreatic cancer growth[13]. Recent advancements in single-cell RNA sequencing (scRNA-seq) have provided an unprecedented understanding of tumor heterogeneity in the PDAC microenvironment[14–16]. Steele et al. described the immune characteristics of PDAC in-depth via multiple complementary approaches, including mass cytometry, scRNA-seq and multiplex fluorescent immunohistochemistry (mfIHC)[17]. Chen et al. discovered a novel subset of cancer-associated fibroblasts (CAFs), which they termed complement-secreting CAFs (csCAFs). They also reported significant alterations in the proportion and gene expression profile of ductal cells and immune cells from early to late-stage PDAC[18]. The diverse subclusters of TANs, each with distinct functions, have been thoroughly reported in liver cancer[19], non-

[1]Department of Abdominal Oncology, the Cancer Center of the Fifth Affiliated Hospital of Sun Yat-sen University, Zhuhai, Guangdong, China. [2]Department of Oncology, Fujian Provincial Hospital, Fuzhou University Affiliated Provincial Hospital, Fuzhou, Fujian, China. [3]These authors contributed equally: Yan Zeng, Jiaping Yu, Yutong Chen. ✉e-mail: chenshli7@mail.sysu.edu.cn; pwenzh@mail.sysu.edu.cn; zenglinj@mail.sysu.edu.cn

THE HORMEL INSTITUTE
UNIVERSITY OF MINNESOTA

small cell lung cancer (NSCLC)[20], and squamous cell carcinoma[21]. Wu et al. integrated the neutrophil transcriptomes of 225 samples from 143 patients across 17 cancer types and observed transcriptional heterogeneity related to 10 cell states. To our knowledge, this is the most comprehensive study associated with TANs[22]. Although previous scRNA-seq studies have revealed the heterogeneity of neutrophils within the PDAC microenvironment, those studies have focused specifically on human neutrophils from tissues and peripheral blood mononuclear cells (PBMCs) from five patients with PDAC[22,23]. The heterogeneity and biological function of TANs in PDAC remain to be elucidated.

In this study, we performed scRNA-seq analysis, identified distinct seven subtypes of neutrophils in 16 PDAC samples and three adjacent normal pancreas samples and further confirmed the existence of these neutrophil subclusters with additional data from 27 PDAC patients. We highlighted and validated the features of novel MIF+ TANs and subsequently explored their protumor functions and underlying mechanisms.

Results

Single-cell landscape of neutrophils in PDAC

To thoroughly catalog the heterogeneity of neutrophils in PDAC, we used published scRNA-seq data on 16 PDAC tissue samples, three adjacent normal pancreas samples, 16 PBMC samples isolated from human PDAC patients, and four PBMC samples isolated from healthy volunteers. After initial quality control, we batch-corrected the data (Supplementary Fig. 1A–B) and subsequently used dimensionality reduction and clustering through uniform manifold approximation and projection (UMAP) (Supplementary Fig. 1C). We classified a total of 51,136 cells into 18 cell clusters on the basis of published lineage markers (Supplementary Fig. 1D). The above procedures were also performed in PBMC samples (Supplementary Fig. 2). To gain deeper insight into the heterogeneity of neutrophils, we separated neutrophils and reperformed dimensionality reduction and clustering. Five neutrophil subclusters in peripheral blood and seven neutrophil subclusters in tumors were identified (Fig. 1A, B). Neu_06_OLR1 and Neu_07_MIF were exclusively found in tumors and designated as TANs; the other five subsets (Neu_01_AIF1, Neu_02_S100A12, Neu_03_MMP9, Neu_04_STAT1 and Neu_05_IFIT1) were enriched in both the tumor and peripheral blood. There were also no differences in the proportions of these five neutrophil subpopulations between the peripheral blood of healthy volunteers and PDAC patients. Correlation analysis revealed that two TAN subtypes were more distinct from the other five clusters, which presented very similar expression profiles (Fig. 1C, Supplementary Tables 1–2). We further investigated the features of each neutrophil subcluster and observed distinct gene signatures (Fig. 1D, E, Supplementary Fig. 3A–B, Supplementary Tables 3–4). Notably, characteristic genes defining the Neu_01_AIF1 subcluster showed relatively higher expression across other neutrophil subpopulations, suggesting conserved functional roles in neutrophil biology. Neu_02_S100A12 was characterized by high expression of genes associated with activated proinflammatory neutrophils, including S100A12, CST7 and MME. The Neu_03_MMP9 subset was similar to the Neu_02_S100A12 subset in terms of expression profile but exhibited upregulated expression of neutrophil extracellular trap (NET)-associated genes, including MMP9 and S100P. Neu_04_STAT1 and Neu_05_IFIT1 exhibited a unique transcriptional signature related to the expression of interferon-stimulated genes. Neu_04_STAT1 highly expressed STAT1, GBP1 and GBP5, whereas Neu_05_IFIT1 highly expressed IFIT1, ISG15 and RSAD2. In addition, Neu_05_IFIT1 exhibited upregulated expression of CD274 (Supplementary Fig. 3C). Compared to the other clusters, Neu_06_OLR1 exhibited differential expression of the putative marker of polymorphonuclear myeloid-derived suppressor cells (PMN-MDSCs) OLR1 and the proinflammatory cytokine CCL4. Neu_07_MIF was characterized as a protumor subcluster that expressed a variety of protumor molecules, such as MIF and the proangiogenic factor VEGFA. In addition, the Neu_07_MIF subcluster exhibited a chronically activated/aged/exhausted TAN phenotype, which is characterized by downregulated expression of SELL and CXCR2 (both markers suppressed in aged

neutrophils), along with upregulated expression of the activation/exhaustion-associated markers CD83 (an inhibitory immune checkpoint), CXCR4, CCRL2 (the atypical chemokine receptor), and C15orf48 (a mitochondrial transcript upregulated during inflammation)[20]. To further validate the existence of these neutrophil subclusters, we analyzed additional data from 27 PDAC patients and identified five neutrophil subclusters: AIF1+ neutrophils, MMP9+ neutrophils, STAT1+ neutrophils, OLR1+ neutrophils and MIF+ neutrophils (Fig. 1F, G, Supplementary Fig. 3D, Supplementary Table 5). Furthermore, we assessed the correlations between our neutrophil subclusters and those reported in four independent studies[19,20,22,23] (Supplementary Fig. 3E).

Prognosis evaluation and pseudotime trajectory analysis of neutrophil subclusters in PDAC

To evaluate the clinical relevance of the neutrophil subclusters, we integrated RNA-seq and survival data from the TCGA-PAAD cohort. Survival analysis revealed that the Neu_04_STAT1, Neu_06_OLR1 and Neu_07_MIF subclusters were associated with poorer prognosis in pancreatic cancer (Supplementary Fig. 4A, Supplementary Table 6). To further investigate their prognostic role in PDAC, we performed survival analysis restricted to PDAC patients in the TCGA-PAAD cohort. Only Neu_07_MIF subcluster was significantly associated with reduced overall survival among PDAC patients (Fig. 2A–G). Neu_07_MIF subcluster also demonstrated significant association with poor prognosis in univariate Cox analysis (HR = 2.102, $p = 0.028$). After adjusting for clinicopathological variables including age and sex in multivariate analysis, Neu_07_MIF subcluster remained an independent prognostic factor (HR = 2.094, 95% CI: 1.081–4.058, $p = 0.029$; Supplementary Fig. 4B). To delve deeper into the dynamic transition of neutrophils from the peripheral blood to the PDAC microenvironment, we utilized Monocle 3 to illustrate the pseudotime trajectory of neutrophils. The trajectory began with Neu_01_AIF1, which subsequently differentiated into two states. In the first state, Neu_01_AIF1 transitioned to Neu_02_S100A12 and Neu_03_MMP9. In another state, Neu_01_AIF1 differentiated into an intermediate state, Neu_04_STAT1, and subsequently transitioned to Neu_05_IFIT1 and Neu_06_OLR1. Neu_06_OLR1 ultimately differentiated into Neu_07_MIF (Fig. 2H). We further identified genes with conserved expression patterns in neutrophils and found that the canonical neutrophil markers S100A8, S100A9, and CXCR2 were significantly downregulated along the developmental trajectory. The expression of CXCR4 initially decreased but subsequently increased, consistent with neutrophil developmental patterns (Fig. 2I, J, Supplementary Table 7). Additionally, Neu_06_OLR1 and Neu_07_MIF presented elevated expression of their respective marker genes, OLR1 and MIF.

The function of neutrophil subclusters in PDAC

On the basis of the reported roles of hypoxia[24], NET[25] and ferroptosis[26] as distinct mechanisms of neutrophils in the TME, we analyzed the defining characteristics of neutrophil subclusters (Supplementary Table 8). Compared with the other neutrophil subclusters, Neu_07_MIF presented the highest scores for hypoxia and ferroptosis. Compared with the other neutrophil subclusters, the Neu_02_S100A12 and Neu_03_MMP9 subclusters had higher NET scores (Fig. 3A). We further performed GSVA to delineate the functional profiles of neutrophil subclusters in PDAC (Fig. 3B, Supplementary Table 9). Pathway enrichment analysis indicated that Neu_05_IFIT1 was strongly associated with the interferon alpha response pathway. Neu_06_OLR1 preferentially exhibited increased enrichment of cell cycle-related gene sets, including those related to E2F targets, the G2M checkpoint, and TNFA signaling via the NF-KB pathway, suggesting early activation of TANs in the TME. Neu_07_MIF exhibited enrichment of genes related to cholesterol homeostasis, hypoxia and the oxidative phosphorylation pathway. To further characterize Neu_07_MIF, we compared it with Neu_06_OLR1 and identified 72 upregulated and 156 downregulated genes (Fig. 3C, Supplementary Table 10). Compared with Neu_06_OLR1, Neu_07_MIF was notably enriched in hypoxic metabolism-related
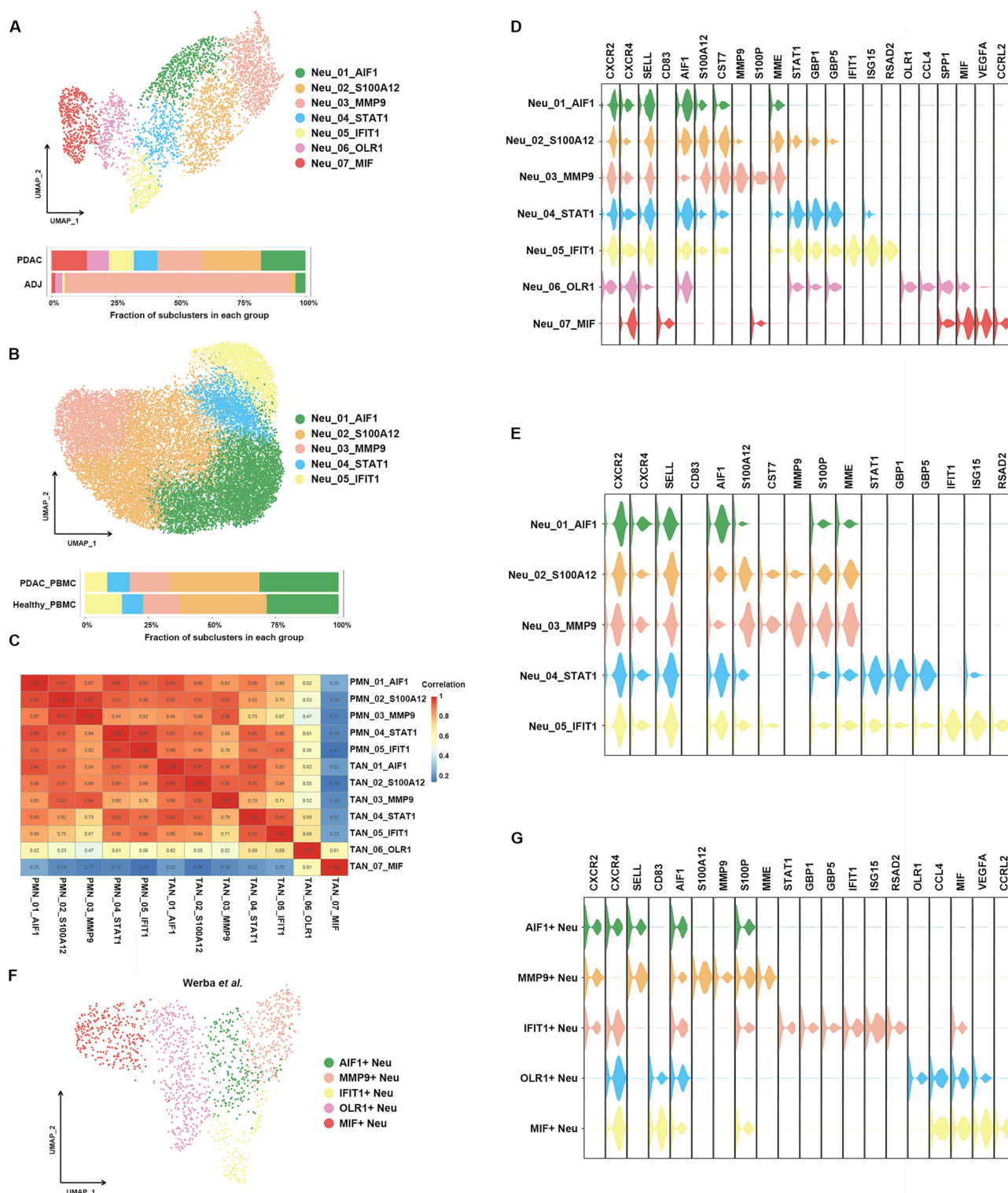
Fig. 1 | Single-cell landscape of neutrophils from PDAC. A UMAP plot showing neutrophil subclusters from 16 PDAC tissues and three adjacent normal pancreas samples. The relative proportion of each cell cluster is indicated. **B** UMAP plot showing neutrophil subclusters from 20 PBMC samples, including 16 PDAC patient samples and four healthy donor samples. The relative proportion of each cell cluster is indicated. **C** Spearman's correlation coefficients were calculated to measure the relationships between neutrophil subclusters in peripheral blood and those in tumors. The average expression of the top 1000 genes with the largest standard deviation in each subcluster was calculated, followed by Spearman's correlation analysis. **D, E** Violin plots showing marker genes of neutrophil subclusters. **F** UMAP plot showing neutrophil subclusters from 27 PDAC tissues. **G** Violin plots illustrating marker genes of neutrophil subclusters. Neu neutrophils, ADJ adjacent normal samples, PMN neutrophils in peripheral blood, TAN neutrophils in tumors.
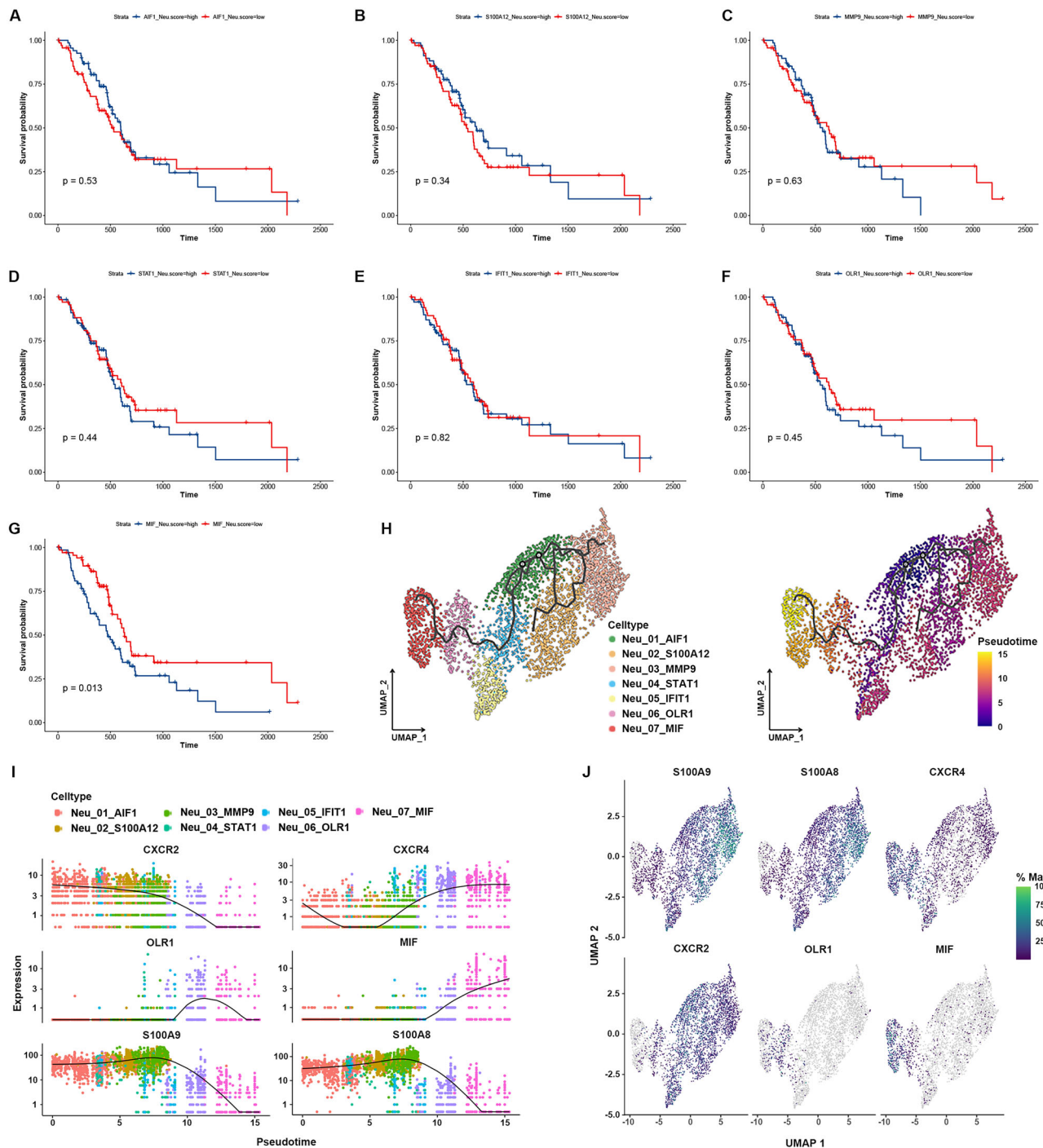
Fig. 2 | **Prognosis evaluation and pseudotime trajectory analysis of neutrophil subclusters in PDAC. A–G** Kaplan–Meier survival curves illustrating the overall survival of 141 PDAC patients in the TCGA-PAAD cohort. The patients were equally divided into two groups on the basis of the score of the neutrophil subcluster signature. The score was assessed by GSVA. **H** Pseudotime trajectory analysis showing the differentiation of neutrophils. Left: Each point was a cell and was assigned a color on the basis of its subcluster. Right: Each point was a cell and was assigned a color on the basis of its pseudotime value. **I, J** Plots displaying the pseudotime-ordered expression and transcript accumulation of selected genes. *$p < 0.05$; **$p < 0.01$; ***$p < 0.001$.

signaling pathways, including oxidative phosphorylation, glycolysis and the hypoxia pathway (Fig. 3D, Supplementary Table 11). Conversely, compared with Neu_07_MIF, Neu_06_OLR1 was enriched in genes related to neutrophil immune functions, including the interferon gamma response, inflammatory response and interferon alpha response pathways. Moreover, we analyzed the differentially expressed genes between the Neu_05_IFIT1 and Neu_04_STAT1 subclusters. Interestingly, Neu_05_IFIT1 exhibited greater enrichment of genes related to the glycolysis and hypoxia pathways than Neu_04_STAT1 (Fig. 3E, F, Supplementary Tables 12–13). These

results indicate that the phenotypes of neutrophils are dynamically modulated by local cues present in the TME.

Cell–cell communication analysis and transcription factor analysis of neutrophil subclusters in PDAC

To explore the interactions between neutrophils and other cells in the PDAC microenvironment, we employed CellChat to infer cellular interactions on the basis of a ligand–receptor signaling database (Supplementary Fig. 4C). Cell–cell communication analysis revealed that neutrophils demonstrated
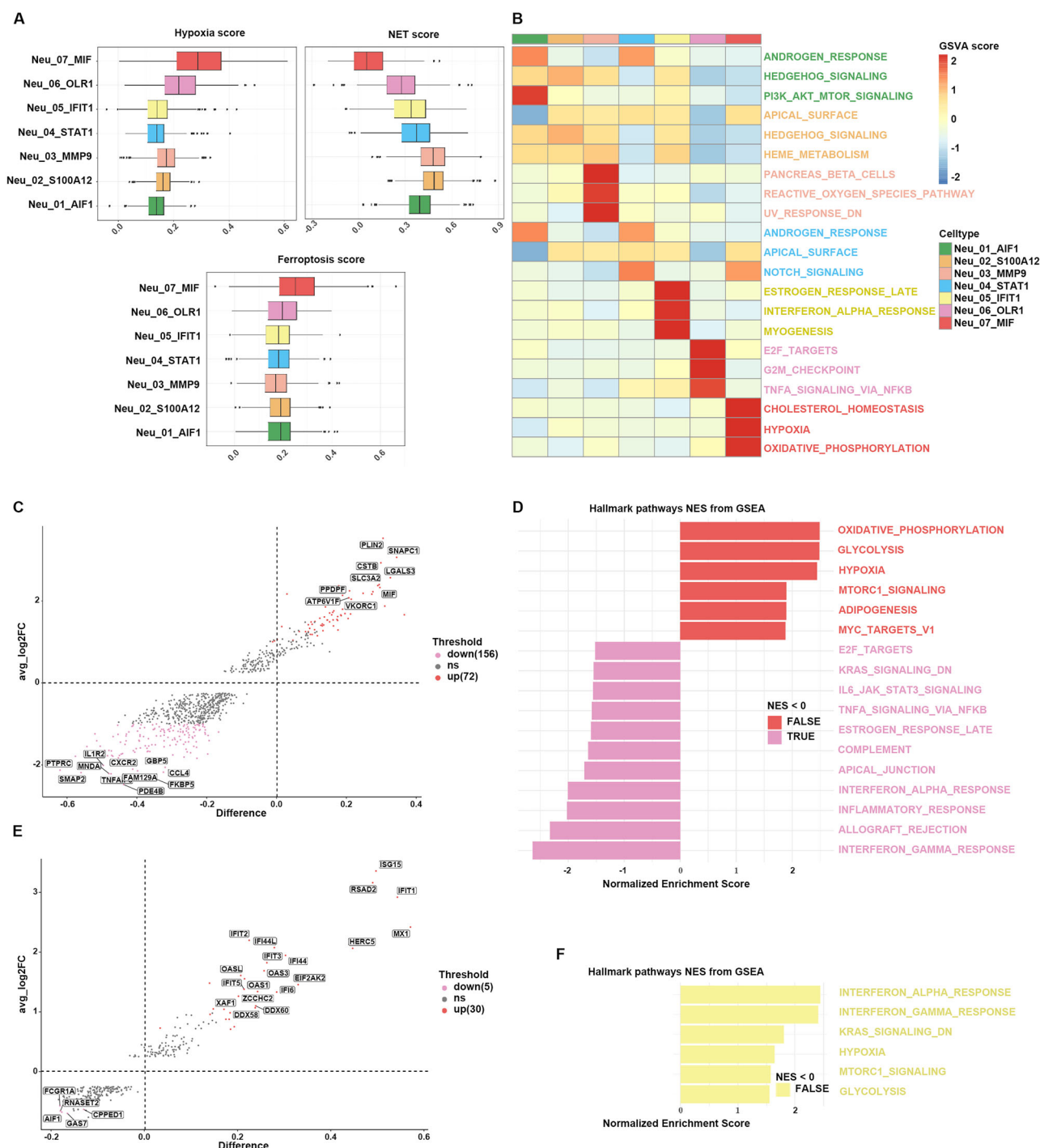
Fig. 3 | The functions of neutrophil subclusters in PDAC. A Box plots showing the scores for hypoxia, neutrophil extracellular trap (NET) and ferroptosis in each neutrophil subcluster. **B** Heatmap illustrating the differences in 50 hallmark pathways of each neutrophil subcluster according to GSVA. **C** Scatter plot showing the differentially expressed genes (DEGs) between Neu_07_MIF and Neu_06_OLR1. The x-axis represents the difference in the percentage of cells expressing DEGs. The selection criteria for DEGs were as follows: abs(log2FC) > 1 and adjusted p < 0.05.

D Bar plot showing the differences in 50 hallmark pathways between Neu_07_MIF and Neu_06_OLR1 through GSEA. **E** Scatter plot showing the DEGs between Neu_05_IFIT1 and Neu_04_STAT1. The selection criteria for differential genes were as follows: abs(log2FC) > 0.5 and adjusted p < 0.05. **F** Bar plot depicting the differences in 50 hallmark pathways between Neu_05_IFITM1 and Neu_04_STAT1 through GSEA.

the strongest interactions with macrophages and monocytes, in terms of both number and strength (Supplementary Fig. 4D). The key ligand–receptor pairs between neutrophils and other cells are displayed in Supplementary Fig. 4E. To further investigate the interplay between neutrophils and other immune cells in the PDAC microenvironment, immune cells from the scRNA-seq dataset were reclustered and reanalyzed (Supplementary Fig. 5A–B, Supplementary Table 14). Cell–cell communication

analysis between neutrophil subclusters and other immune cells revealed that MIF+ neutrophils presented the highest interaction frequency, and which the MIF and SPP1 signaling pathways were highly active in these cells (Fig. 4A, B). The detailed gene expression profiles of these cells are displayed in Supplementary Fig. 5C. Compared with other T-cell subsets, MIF+ neutrophils exhibited stronger interactions with FOXP3 + CD4 + T cells. The key ligand–receptor pairs between MIF+ neutrophils and other
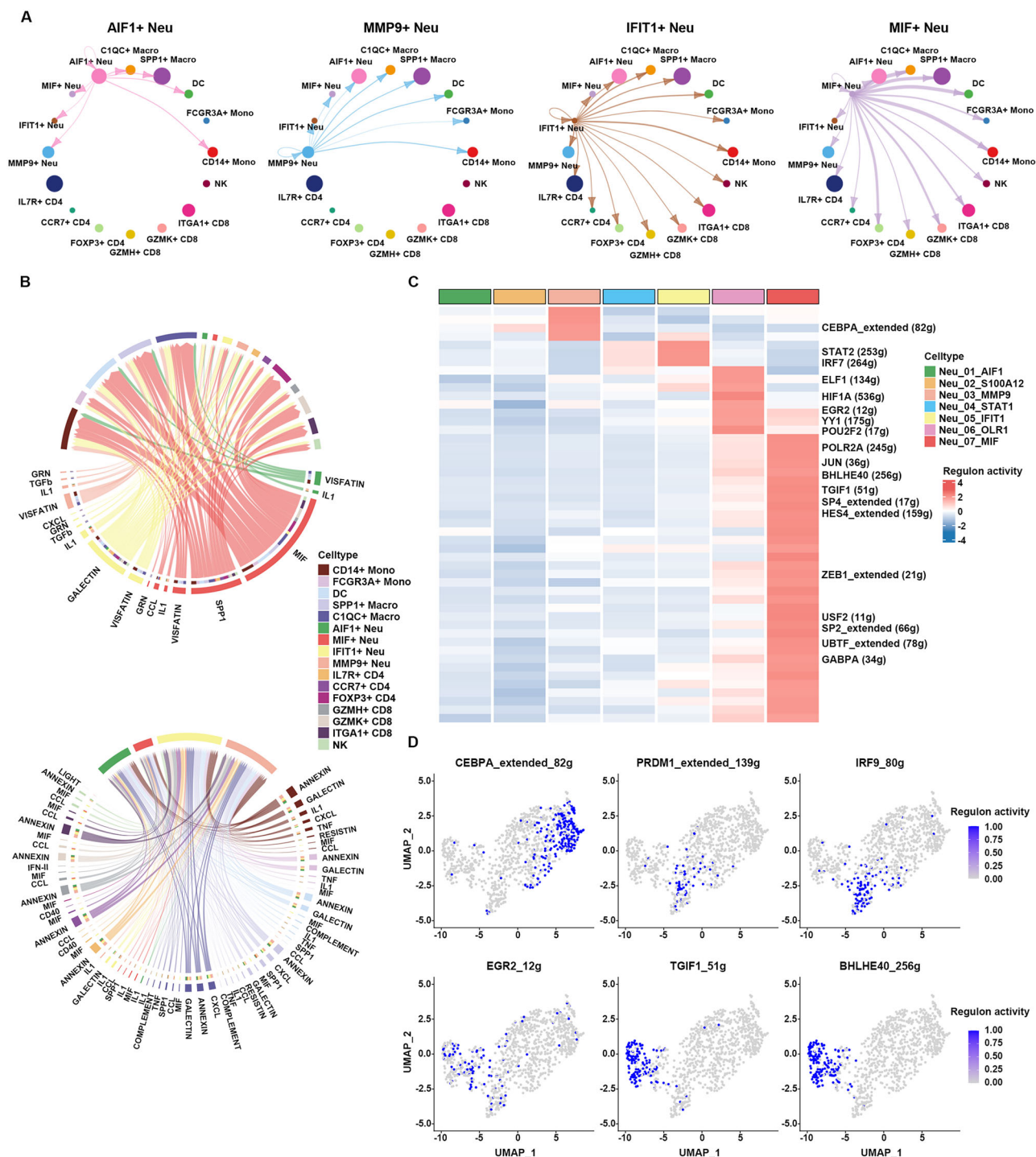
Fig. 4 | Cell−cell communication analysis and transcription factor analysis of neutrophil subclusters in PDAC. A Chord plots showing the strength of outgoing events in interactions between neutrophils and other immune cell subclusters. **B** Chord plots illustrating the significant pathways annotated as "Secreted Signaling" between neutrophil and other immune cell subclusters. Chords extend from the neutrophil ligand source to other immune cells expressing their partner receptor (up). Chords point from the other immune cell ligand source to neutrophils expressing their partner receptor (down). The color of each chord represents different cell clusters, and the length of the chord indicates the interaction strength. **C** A heatmap showing the differences in transcription factor activity across neutrophil clusters, as scored by SCENIC. Transcription factor activity levels are represented with colors. **D** UMAP plots depicting the binary regulon activity of important transcription factors. The states of the transcription factors in each cell class are indicated in blue for active states and white for inactive states.

immune cells were MIF-CD74/CXCR4 and MIF-CD74/CD44, while LGALS9−CD45 and LGALS9−CD44 were prominent ligand−receptor pairs between IFIT1+ neutrophils and other immune cells. Conversely, IFIT1+ and MMP9+ neutrophils receive more incoming signals from other immune cells. Additionally, other immune cells attracted neutrophils via the ANXA1-FPR1 axis (Supplementary Fig. 5D). To further investigate

transcriptomic differences and transcription factor motifs across neutrophil subclusters, we performed SCENIC analysis. The results revealed that regulon activity aligned with the transcriptomic classification of neutrophil subclusters (Fig. 4C, D, Supplementary Fig. 5E). Neu_03_MMP9 exhibited elevated CUX1 and CEBPA regulon activity, whereas the PRDM1, IRF7 and STAT2 regulons were more active in Neu_04_STAT1 and Neu_05_IFIT1.

POU2F2, EGR2, and HIF1A regulons were activated in Neu_06_OLR1 and possibly associated with neutrophil reprogramming in the PDAC microenvironment. The core transcription motifs of TGIF1, HES4, BHLHE40, ZEB1, JUN, and POLR2A were activated in Neu_07_MIF, which are involved in tumor-promoting pathways.

Reprogramming of neutrophils in PDAC

To further validate the presence of the novel OLR1+ and MIF+ TAN subsets, we performed IF staining in 10 PDAC tissues and detected OLR1+ TANs in all 10 samples and MIF+ TANs in 7 samples (Fig. 5A, B, Supplementary Fig. 6A). In the orthotopic pancreatic tumor and orthotopic patient-derived xenograft (PDX) models, MIF expression was predominantly localized to a distinct population of tumor-infiltrating neutrophils, whereas minimal expression was observed in neutrophils from bone marrow and spleen (Fig. 5C–E, Supplementary Fig. 6B). The consistent MIF expression in tumor-infiltrating neutrophils across various tumor models suggests that MIF could serve as a potential biomarker for TANs. To clarify whether tumor cells can directly induce the reprogramming of neutrophils, we isolated neutrophils from bone marrow of mice and cultured them separately in two types of tumor conditioned medium (TCM). After 2 days, neutrophils cultured in TCM presented increased expression of MIF, whereas those cultured in control medium did not show the same effect (Fig. 5F–H).

MIF+ TANs promoted PDAC progression through the activation of the ERK and AKT pathways and EMT

We treated HL-60 cells with 1.25% DMSO to induce dHL-60 cells and subsequently assessed the expression of CD66b and CD11b (Supplementary Fig. 6C–E). To investigate the role of MIF+ TANs, we overexpressed MIF in dHL-60 cells and cocultured them with PDAC cells (AsPC-1, PANC-1, and CFPAC-1 cells). qRT-PCR and ELISA were performed to verify the transfection efficiency (Supplementary Fig. 6F–G). CCK-8, EdU and colony formation assays were employed to evaluate cell viability. The results demonstrated that the proliferative capacity of PDAC cells improved after coculture with MIF-overexpressing dHL-60 cells (Fig. 6A–E). Moreover, wound-healing and transwell assays revealed increased migratory capacity of PDAC cells after coculture (Fig. 6F–I). These results revealed that MIF-overexpressing dHL-60 cells promoted the proliferation and migration of PDAC cells. On the basis of previous studies indicating that the MAPK/ERK and PI3K/AKT pathways and EMT are involved in MIF-mediated cellular functions[27,28], we analyzed the expression of these signaling pathway markers in PDAC cells. The levels of phosphorylated ERK1/2 (p-ERK1/2) and phosphorylated AKT (p-AKT) in PDAC cells increased after coculture with MIF-overexpressing dHL-60 cells, whereas total ERK1/2 and total AKT levels remained unaffected (Fig. 6J–L). Furthermore, E-cadherin expression decreased alongside elevated vimentin and N-cadherin expression in PDAC cells after coculture (Fig. 6M).

MIF inhibition reversed MIF+ TANs-driven PDAC progression

To investigate whether the protumorigenic effects of MIF+ TANs rely on MIF activity, we treated coculture systems with the MIF inhibitor 4-iodo-6-phenylpyrimidine (4-IPP). We first established the dose−response relationship of 4-IPP in PDAC cells, with half-maximal inhibitory concentration (IC50) values of 54 μM (AsPC-1), 98 μM (PANC-1), and 24 μM (CFPAC-1) after 48 h of treatment (Supplementary Fig. 6H). 4-IPP administration abolished the enhanced proliferative capacity of PDAC cells induced by MIF-overexpressing dHL-60 cells, as evidenced by CCK-8 and colony formation assays (Fig. 7A–C). Similarly, the promigratory effects of MIF-overexpressing dHL-60 cells on PDAC cells were significantly attenuated upon 4-IPP treatment; wound closure rates decreased, and transwell migration was suppressed (Fig. 7D–G). Mechanistically, 4-IPP suppressed the activation of the MAPK/ERK and PI3K/AKT pathways in PDAC cells, as demonstrated by decreased phosphorylation levels of ERK1/2 and AKT, without altering total ERK1/2 or AKT expression (Fig. 7H–J). Furthermore, the EMT-promoting effects in MIF-overexpressing dHL-60 cells were

reversed by 4-IPP treatment, which was characterized by restored E-cadherin expression and reduced vimentin and N-cadherin levels in PDAC cells (Fig. 7K). These results collectively indicate that pharmacological inhibition of MIF abrogates MIF+ TANs-mediated tumor-promoting functions, highlighting MIF as a critical mediator of TANs-driven PDAC progression. The study design and schematic diagram are shown in Fig. 8.

Discussion

In a variety of human tumors, including PDAC, a high degree of TAN infiltration is associated with a poor prognosis[29]. Since its emergence, scRNA-seq has facilitated the characterization of distinct immune profiles and led to a comprehensive understanding of the PDAC microenvironment[16]. Our study aimed to expand the understanding of neutrophil heterogeneity in the PDAC microenvironment at single-cell resolution, pinpoint distinct subclusters that play a role in tumor progression, and explore the fundamental mechanisms that steer neutrophils toward protumor phenotypes.

In this study, seven subclusters of human neutrophils were identified in PDAC. AIF1+ neutrophils, S100A12+ neutrophils, MMP9+ neutrophils, STAT1+ neutrophils and IFIT1+ neutrophils were found in both the tumor and peripheral blood. There were no differences in the percentage of each neutrophil subcluster in the peripheral blood between healthy individuals and PDAC patients, which is consistent with previous reports[23]. Another two subsets, OLR1+ neutrophils and MIF+ neutrophils, were exclusively found in the tumor and were thus classified as TANs. AIF1+ neutrophils without specific features exhibited the initial phenotype. S100A12+ and MMP9+ neutrophils have been reported in NSCLC[20] and liver cancer[19]. MMP9+ neutrophils in PDAC express minimal amounts of MMP8, while MMP8 is a significantly upregulated marker of MMP9+ neutrophils in liver cancer[19]. These results suggest that highly similar cell subpopulations across various tumors possess distinct genes and functions. IFIT1+ neutrophils and intermediate-state STAT1+ neutrophils demonstrated robust expression of interferon-stimulated genes. IFIT1+ neutrophils in liver cancer distinctly express PD-L1[19]. In our study, IFIT1+ and STAT1+ neutrophils also presented increased PD-L1 expression. OLR1+ TANs in PDAC highly expressed OLR1 and CCL4, which closely resembled CCL4+ TANs in liver cancer. CCL4+ TANs can recruit macrophages in vitro[19]. OLR1 has emerged as one of the most significantly overexpressed genes in PMN-MDSCs[30]. Further research on OLR1+ TANs may clarify the differences between TANs and MDSCs to facilitate their identification in subsequent studies. MIF+ TANs represent a typical procarcinogenic neutrophil subcluster. This subcluster overexpresses classical procarcinogenic genes and is associated with hypoxia and glycolysis, which has been reported in liver cancer[19], NSCLC[20] and PDAC[23]. In addition to previously reported genes, including VEGFA, LGALS3, PLAU, and SPP1, we identified MIF as one of the top upregulated genes in TANs. We further found that MIF was also one of the top upregulated genes in dcTRAIL-R1+ neutrophils[31] and VEGFA + SPP1+ neutrophils[22], the terminal procarcinogenic neutrophil subclusters identified in different studies. Although these studies did not focus on the expression and function of MIF in TANs, MIF may be a specific marker gene for TANs. Interestingly, MIF+ TANs exhibited upregulated expression of CCRL2, which can enhance the antitumor T-cell response[32] and promote NK-cell-mediated immune surveillance. The transcriptional landscapes of neutrophil subclusters underscore their dynamic plasticity in the PDAC microenvironment.

The phenotype of neutrophils varies depending on temporal, spatial and disease-specific cues and their developmental progression includes transitions from bone marrow-resident immature cells (characterized by high CXCR4, low CXCR2, and low MME expression) to circulating mature cells (marked by high CXCR2 and SELL expression), culminating in an aged or senescent state (noted in high CXCR4 expression)[33,34]. The pseudotime trajectory analysis unveiled a continuum of neutrophil transitional states within the PDAC microenvironment, matching the developmental patterns of neutrophil. Throughout this developmental process, TANs predominantly exhibit an aged/senescent phenotype and lose classical
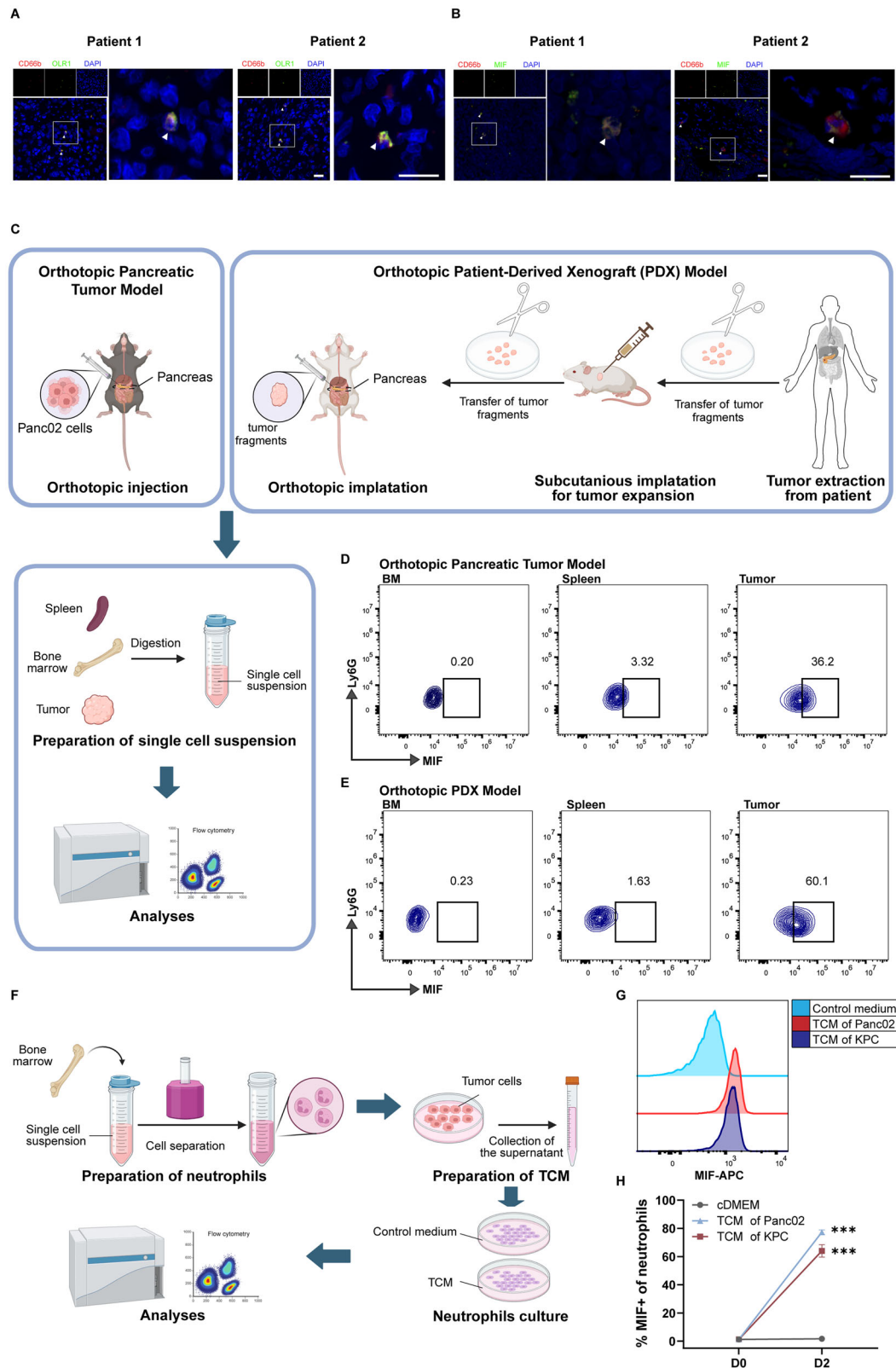
Fig. 5 | Reprogramming of neutrophils in PDAC. A, B Images of IF staining for OLR1+ and MIF+ TANs in human PDAC tissues are presented. Nuclei were stained with DAPI. The scale bar is 20 μm. **C** Schematic workflow of the orthotopic pancreatic tumor model and PDX model. Neutrophils from bone marrow, spleen, and pancreatic tumors of tumor-bearing mice were used for flow cytometry. **D, E** Representative flow cytometry plots illustrating MIF expression in Ly6G+ neutrophils within bone marrow, spleen, and tumor. MIF expression specifically identified a distinct subset of tumor-infiltrating neutrophils. **F** Experimental setup involving the in vitro culture of sorted neutrophils from wild-type mouse bone marrow in cDMEM compared with TCM. **G** Representative flow cytometry plots showing that the expression of MIF increased in sorted neutrophils after 2 days of culture in TCM but not in control medium. **H** Neutrophils cultured in TCM upregulated MIF over time. Line plots show the percentage of MIF+ cells in the neutrophil population. Schematic diagrams were created with BioRender.com. *$p < 0.05$; **$p < 0.01$; ***$p < 0.001$. PDX patient-derived xenograft, TCM tumor-conditioned medium.
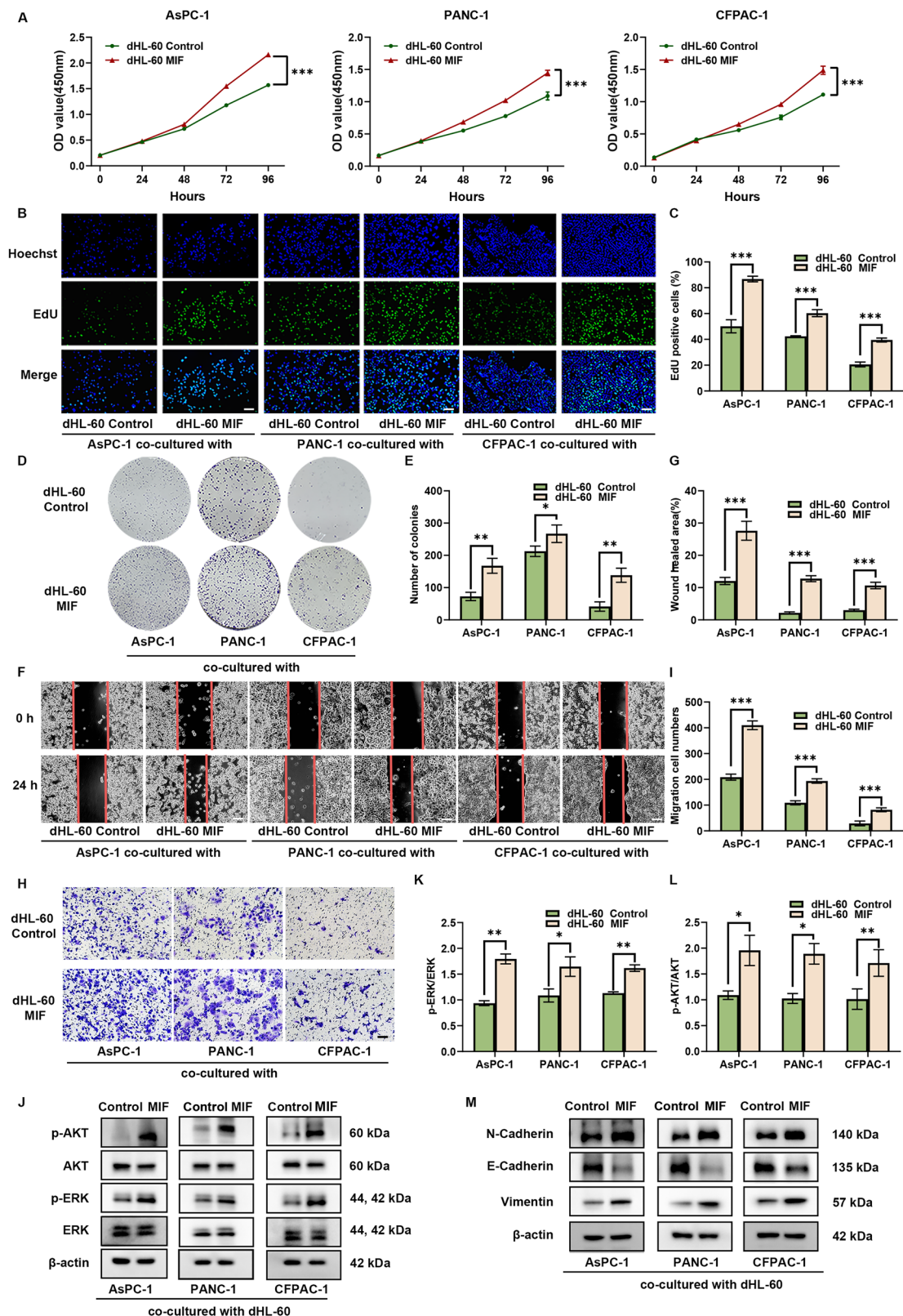
Fig. 6 | MIF+ TANs promoted PDAC progression through the activation of the ERK and AKT pathways and EMT. PDAC cells (AsPC-1, PANC-1, and CFPAC-1 cells) were cocultured with MIF-overexpressing dHL-60 cells or control cells. **A** To evaluate the proliferative ability of PDAC cells, CCK-8 assays were performed. **B**, **C** EdU assays were performed to evaluate the proliferative ability of PDAC cells. **D**, **E** Colony formation assays were performed to evaluate the proliferative ability of PDAC cells. **F**, **G** Wound healing assays were conducted to detect the migratory ability of PDAC cells. The scale bar is 100 μm. **H**, **I** Transwell assays were conducted to detect the migratory ability of PDAC cells. The scale bar is 100 μm. **J**–**L** The expression of ERK, p-ERK, AKT and p-AKT in PDAC cells was detected by western blotting. **M** The expression of EMT markers (E-cadherin, vimentin, and N-cadherin) in PDAC cells was detected by western blotting. The data are representative of three independent experiments. *$p < 0.05$; **$p < 0.01$; ***$p < 0.001$.
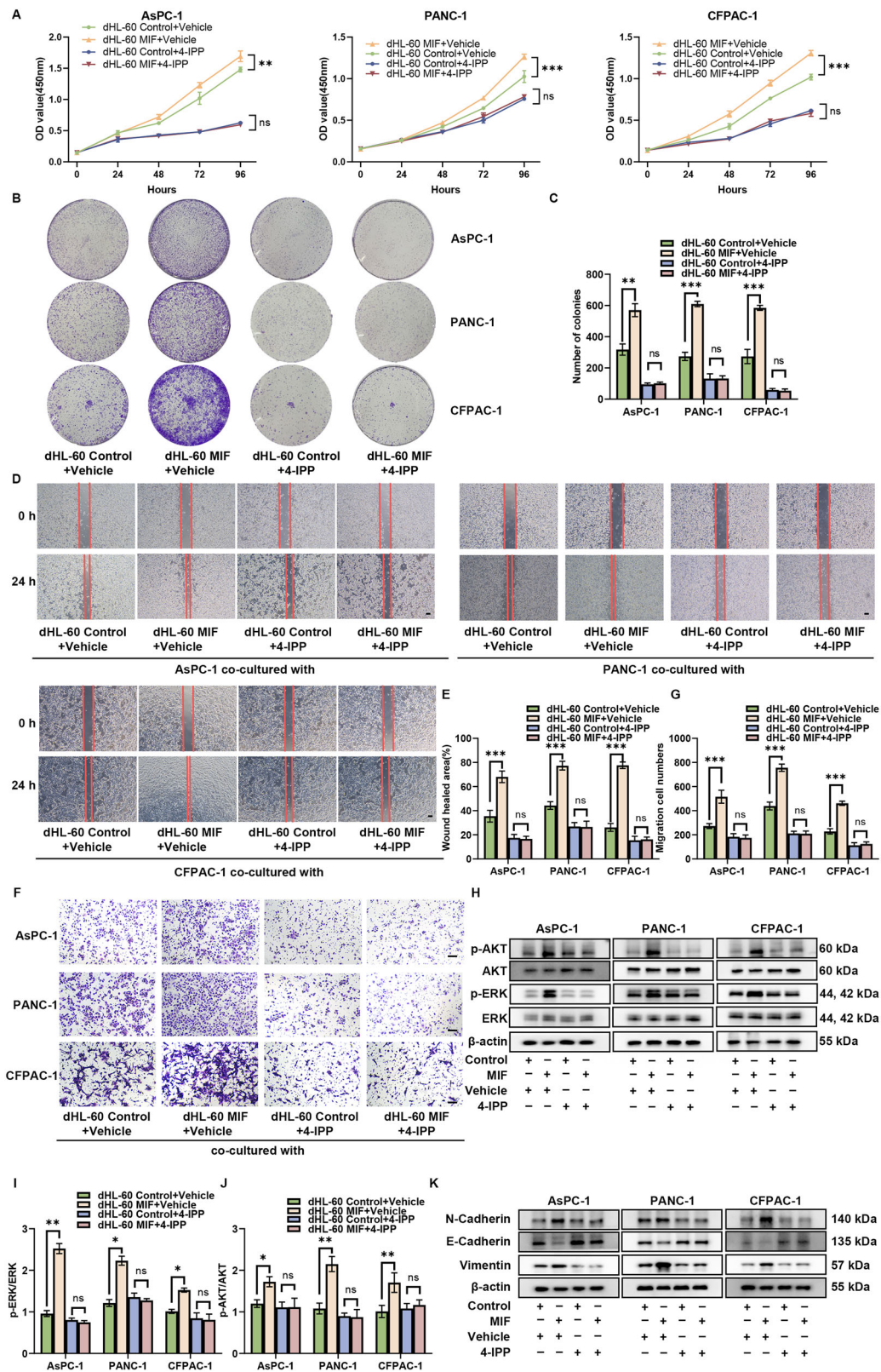
Fig. 7 | MIF inhibition by 4-IPP reversed MIF+ TANs-driven PDAC progression. **A–C** Proliferative capacity of PDAC cells in coculture systems treated with 4-IPP or vehicle, as assessed by CCK-8 and colony formation assays. **D, E** Migratory capabilities of PDAC cells in coculture systems treated with 4-IPP or vehicle, as evaluated by wound healing assays. The scale bar is 100 μm. **F, G** Migratory capabilities of PDAC cells in coculture systems treated with 4-IPP or vehicle, as evaluated by transwell assays. The scale bar is 100 μm. **H–J** Western blotting analysis of ERK, p-ERK, AKT, and p-AKT expression in PDAC cells. **K** Western blotting analysis of EMT markers in PDAC cells. The data are representative of three independent experiments. *$p < 0.05$; **$p < 0.01$; ***$p < 0.001$.
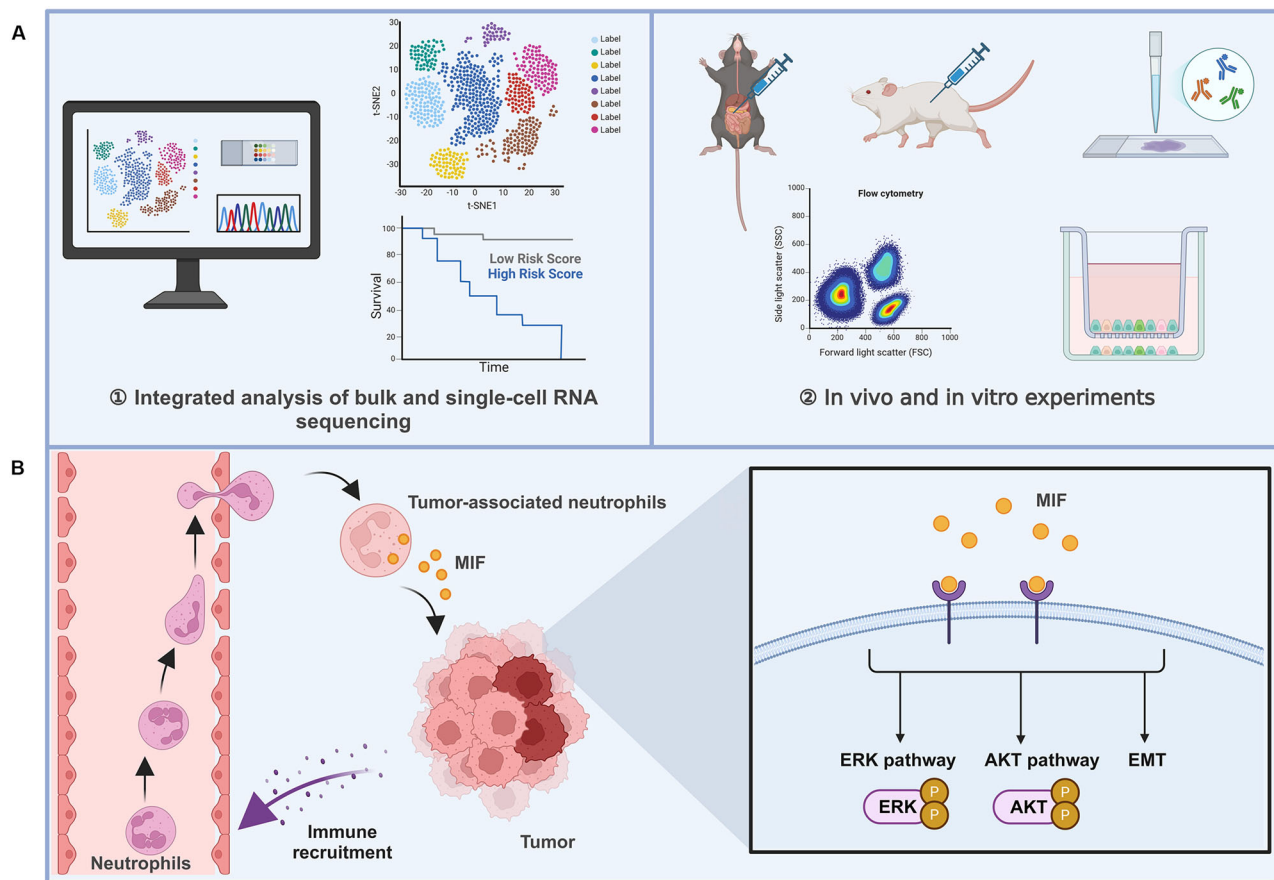
Fig. 8 | Study design and schematic diagram. A Study design of neutrophil heterogeneity in PDAC. **B** Schematic diagram of the mechanism by which MIF+ TANs promote PDAC progression through the activation of the ERK and AKT pathways and EMT. This illustration was created with BioRender.com.

neutrophil markers, including S100A8 and S100A9. Notably, TANs exhibited robust downregulation of CXCR2, which is consistent with prior reports[33]. CXCR2 expressed on neutrophils is critical for their recruitment to the TME. Preclinical studies have demonstrated that blocking CXCR2-mediated neutrophil recruitment suppresses tumor growth and progression across multiple cancer models[8,35,36]. However, the inability of CXCR2 inhibitors to reduce TAN infiltration or alter their activation state may underlie their limited clinical efficacy. Reprogramming neutrophil functionality within the TME remains challenging. Combinatorial strategies targeting both CXCR2 and TAN-specific markers could synergistically enhance therapeutic outcomes. In addition, targeting CXCR4 in murine models has been reported to polarize neutrophils toward an antitumor phenotype[37]. Intercommunication between neutrophils and other cells within the TME has been clarified in recent years. In this study, cell-cell communication analysis revealed that MIF+ TANs expressed high levels of ligands that can bind to other immune cells and modulate their functions. The communication between MIF+ TANs and other immune cells, especially FOXP3+ CD4+ T cells, may contribute to tumor progression. The results of the transcription factor analysis revealed that POU2F2, EGR2 and HIF1A were activated in OLR1+ TANs, potentially contributing to neutrophil reprogramming within the PDAC microenvironment. Conversely, TGIF1, BHLHE40, JUN and POLR2A were activated in MIF+ TANs, further driving TANs toward cancer-promoting phenotypes. The development of effective strategies for reprogramming neutrophils into antitumor states is noteworthy.

MIF is a proinflammatory cytokine with various biological functions that plays crucial roles in the pathogenesis of cancer and inflammatory diseases[27]. Extracellular MIF primarily binds to the cluster of differentiation 74 (CD74)/CD44 complex, thereby activating downstream signaling pathways. MIF has the potential to counteract immunosuppression and

contribute to tumor progression, including tumor proliferation, aggressiveness and angiogenesis[38–40]. It has been reported that MIF is overexpressed in PDAC and is associated with an unfavorable prognosis[28,41–43]. However, its role in neutrophils remains largely unexplored. Although MIF+ TANs have been fully validated in PDAC tissues and orthotopic tumor models, the short lifespan and vulnerability of neutrophils present challenges for conducting in vitro functional studies. To investigate the protumor functions of MIF+ TANs, we used HL-60 cells, which have the capacity to differentiate into a state resembling that of neutrophils after treatment with DMSO[44], to perform experiments. Consistently, we noted a significant increase in both the proliferation and migration of PDAC cells when they were cocultured with dHL-60 cells overexpressing MIF. This observation demonstrates that MIF propels neutrophils toward a protumor subtype. Previous studies have revealed that the MAPK/ERK[45], PI3K/AKT[46,47] and EMT[28] pathways are involved in MIF-mediated cellular functions in PDAC. Our results also demonstrated that MIF+ TANs promote the malignant progression of PDAC via the activation of the ERK and AKT pathways and EMT. Notably, Zhu et al. reported that CD36+ CAFs present elevated MIF expression and recruit CD33+ MDSCs in an MIF-CD74-dependent manner[48]. These findings suggest that MIF inhibition not only directly impedes tumor growth but also remodels the TME. This study reveals MIF as both a defining marker of protumorigenic TANs and a therapeutic target in PDAC.

However, there are some limitations to this study. The original data utilized in this study were based on a limited number of neutrophils from adjacent normal pancreas samples, which precluded a comparison of neutrophils between normal pancreas and PDAC samples. In the section discussing the IFIT1+ neutrophil subcluster, their roles in the peripheral blood from those in the TME remain poorly defined, which has been observed in liver cancer[19]. This group

of neutrophils, which is characterized by the expression of interferon-related genes, warrants further investigation. Although we discovered that MIF+ TANs expressed high levels of ligands that can bind to other immune cells through cell-cell communication analysis, we did not corroborate these results, and further work is needed. A limitation of this study is the absence of techniques such as proteomic analysis and spatial transcriptomics applied to neutrophils. Our team aims to address these aspects in future studies. In addition, we were unable to conduct in vivo experiments to verify the function of MIF+ TANs because of technical limitations in isolating viable MIF+ TANs. This problem can be solved by prolonging the neutrophil half-life, which enables neutrophil transfection. Given that treatment prolongs the neutrophil half-life, more effective neutrophil therapies may be developed in the future.

In summary, our findings provide more insight into the heterogeneity and function of neutrophils in PDAC. We identified two subsets of TANs in the PDAC microenvironment and explored the potential of MIF as a novel biomarker for TANs in PDAC. Our data provide a robust foundation for future investigations that may lead to the identification of novel immunotherapeutic targets for human PDAC.

Methods
Patient samples and ethical authorization
All samples were obtained from PDAC patients who provided informed consent under institutional review board consent protocols at the Fifth Affiliated Hospital of Sun Yat-sen University in Zhuhai, China. This study was authorized by the Ethics Committee of the Fifth Affiliated Hospital of Sun Yat-sen University. The study was conducted in accordance with the Declaration of Helsinki.

scRNA-seq data quality control and analysis
The scRNA-seq data of PDAC were sourced from the Gene Expression Omnibus (GEO) (https://www.ncbi.nlm.nih.gov/geo/), which included the GSE155698 and GSE205013 datasets. We used Seurat (v4.3.0) to process the UMI count matrix. We performed doublet removal by using doubletFinder (v2.0.3). UMIs with excess mitochondrial reads (> 20%), number of features <100 (low read counts) and >10,000 (outliers) were also removed. Subsequently, the matrix was imported into the R package Seurat (v4.3.0) for further analysis. The gene expression levels were normalized and a total of 2000 highly variable genes were generated for performing Principal component analysis (PCA) dimension reduction. We integrated all cells according to sample ID by using harmony. Unsupervised cell clusters were obtained by graph-based clustering approach and visualized by Uniform Manifold Approximation and Projection (UMAP) dimensionality reduction. Unsupervised clustering was performed using Seurat's FindNeighbors (dims = 1:10) and FindClusters (resolution = 0.9) functions. The clusters were annotated to known cell types based on the expression of canonical markers. Marker genes of each cluster were identified using the FindAllMarkers function under the following criteria: min.pct = 0.25 and thresh.use = 0.25. For more detailed annotations, neutrophils were isolated, and the above process was repeated. Unsupervised clustering was performed using Seurat's FindNeighbors and FindClusters functions with the following parameters: for 16 PDAC and three adjacent normal pancreas samples (dims = 1:10, resolution = 0.7); for 20 PBMC samples (dims = 1:10, resolution = 0.6); and for 27 PDAC tissue samples (dims = 1:15, resolution = 0.4). To analyze the correlation between PMN and TAN subpopulations, 1000 genes with the largest standard deviation were extracted from Seurat objects for Spearman analysis. The relevant data mentioned above can be found in Supplementary Data 1.

Pseudotime trajectory analysis
The pseudotime trajectory analysis was conducted using the Monocle 3 package (v1.3.1) in R. This package facilitated the extraction of all neutrophil clusters from scRNA-seq data and the feeding of the gene-cell matrix from the original UMI count scale of these cells into Monocle 3. Differentially

expressed genes along the pseudotime trajectory were identified using the 'graph_test' function with a q-value < 1e-3. These genes were listed in Supplementary Data 1.

Survival analysis
The clinicopathologic characteristics and bulk RNA-seq data of TCGA–PAAD cohort were retrieved from the UCSC Xena database (https://xena.ucsc.edu/). The gene set of neutrophil subclusters was defined based on upregulated genes. These gene sets were included in the Supplementary Data 1. Using gene set variation analysis (GSVA, v1.46.0), patients were divided into two groups based on the median value of the gene set score: high and low. The survival curves of these two groups were compared using the Kaplan–Meier method and log-rank test by R package survival (v3.4-0). Univariate and multivariate Cox regression analyses were performed using the same package.

Functional enrichment analysis
In order to investigate the functions of each neutrophil subcluster, gene sets associated with neutrophil functions were selected. The expression levels of each gene set were estimated for each individual cell using the AddModuleScore function. Gene sets were listed in Supplementary Data 1. In addition, we used UCell (v2.2.0) to quantify the similarities of the neutrophil subpopulation between this study with the previous published articles. The FindMarkers function, gene set enrichment analysis (GSEA, v1.60.0) and GSVA (v1.46.0) were utilized to explore the functional and pathway differences among different neutrophil subclusters. Differentially expressed genes (DEGs) and enrichment results were listed in Supplementary Data 1.

Transcription factor (TF) Analysis
The SCENIC package (v1.3.1) was utilized to identify activated regulons in different neutrophil subsets. The raw count matrix, which served as input, was calculated for co-expression activity using a Spearman correlation by GENIE3 (v1.20.0). These filtered targets were subsequently analyzed for motif enrichment using RcisTarget (v1.18.2). Notably, an AUCell (v1.20.2) with a Wilcoxon rank-sum test was employed to estimate regulatory activity scores for gene motifs located 500 bp upstream of the transcription start sites (TSS) and 10 kb around the TSS. Finally, important regulons modulated by key TFs were identified by Regulon Specificity Score (RSS).

Cell–Cell communication analysis
The R program CellChat (v1.6.1) was employed to infer different cell-to-cell interactions between the neutrophil subclusters and other subclusters, as well as the ligands and receptors for intercellular communication. The Secreted Signaling subset in human databases was selected as the ligand-receptor interaction databases. In accordance with the official procedure, standardized counts were entered into CellChat and standard preprocessing steps were followed.

Immunofluorescence (IF) staining
The slides of PDAC tissues were incubated for 2 h at 65 °C, deparaffinized with xylene and ethanol diluted in a graduated series. Microwave antigen retrieval was carried out using 9% EDTA antigen repair buffer. The slides were blocked with 5% normal goat serum for 1 h at room temperature, followed by overnight incubation with primary antibodies at 4 °C. The slides were incubated with fluorochrome-conjugated secondary antibody for 1 h and DAPI for 5 min. Visualization of the tissue slides was performed using confocal microscopy (Zeiss LSM 900). The antibodies used for IF staining included: CD66b (BioLegend, 305102); MIF (Proteintech, 20415-1-AP); OLR1 (Proteintech, 11837-1-AP); goat-anti-rabbit (Invitrogen, A-11008); and Alexa Fluor® 647 anti-mouse IgM Antibody (BioLegend, 406525).

Orthotopic pancreatic tumor model and orthotopic PDX model
All animal experiments were approved by the Animal Care and Use Committee of Sun Yat-Sen University (Guangzhou, China). Female C57BL/6 mice (6 weeks) were purchased from Zhuhai BesTest Biotech, and female

NOD.Cg-PrkdcscidIl2rgtm1Wjl/SzJ (NSG) mice (6 weeks old) were obtained from Shanghai Model Organisms Center, Inc. For the orthotopic pancreatic tumor model, C57BL/6 mice were administered intrapancreatic injections of Panc02 cells following previously published procedures[31] (n = 3). Briefly, mice were anesthetized by inhalation of isoflurane (2–3% for induction, 1–1.5% for maintenance). A 5 mm vertical midline laparotomy was performed 1 cm caudal to the xiphoid process. The pancreas was exteriorized, and 1×10^5 tumor cells resuspended in PBS and mixed 1:1 with Matrigel (Corning, USA) were injected into the pancreatic body. The pancreas was repositioned within the abdominal cavity, and the incision was closed in layers. Following tumor establishment (3–4 weeks), mice received intraperitoneal D-luciferin and were imaged using an IVIS Lumina Series II imaging system. For the orthotopic PDX model, a viable 2×2 mm portion of tissue was immediately isolated from a surgically resected PDAC specimen and then implanted subcutaneously into NSG mice. After reaching an endpoint of 1.5 cm in maximum diameter, PDX tumors were harvested, minced into 2 mm pieces, and subsequently used to perform orthotopic implantation in NSG mice. At the experimental endpoint, mice were euthanized by CO_2 asphyxiation in a controlled chamber (20–30% volume displacement/min), in accordance with institutional animal care protocols. Neutrophils were isolated from bone marrow, spleen, and tumors of mice bearing orthotopic pancreatic tumors using isolation kits (TBD science, LZS1100P or TBD2013NM), followed by flow cytometry.

Flow cytometry
Cells were harvested in stain buffer (BD Biosciences, USA). For cell-surface staining of dHL-60, cells were performed with CD66b (BioLegend, 305102) for 30 min at 4 °C, followed by Alexa Fluor® 647 anti-mouse IgM Antibody (BioLegend, 406525) for another 30 min at 4 °C. For intracellular staining of neutrophils from mice, cells were first incubated in 0.5 µg Fc Block (BioLegend, 101319) for 10 min, then washed and stained with FITC-conjugated anti-mouse antibodies against Ly-6G (BioLegend, 127605). Stained cells were fixed and permeabilized with BD Cytofix/Cytoperm™ Buffer (BD Biosciences, USA) before secondary stained with CoraLite Plus 647-conjugated MIF Polyclonal antibody (Proteintech, CL647-20415). Flow cytometry analysis was conducted using either a Beckman CytoFlex S flow cytometer. The results were analysed using the FlowJo 10.7 software program.

Cell culture
HL-60, AsPC-1, PANC-1, CFPAC-1 and Panc02 cell lines were obtained from the American Type Culture Collection (ATCC). The KPC cell line (Cat. NO. NM-YD04) was purchased from Shanghai Model Organisms Center, Inc. AsPC-1, PANC-1, CFPAC-1, KPC and Panc02 cell lines were cultured in DMEM medium (Gibco) supplemented with 10% FBS (Gibco) and 1% 100X Pen/Strep (Gibco). HL-60 cells were cultured in RPMI-1640 medium (Gibco) with 10% FBS (Gibco) and 1% 100X Pen/Strep (Gibco). Neutrophil-like differentiated HL-60 (dHL-60) cells were induced by supplementing the culture media of HL-60 with 1.25% DMSO for 5 days. Sorted bone marrow neutrophils through magnetic bead (TBD science, TBD70907-10) were counted, and resuspended at 1×106/ml in control media or TCM.

Cell transfection
The full-length overexpression plasmid of MIF was commercially obtained from MIAOLING BIOLOGY (China). An empty vector was also employed as a negative control. The plasmids were transiently transfected into dHL-60 cells using Lipofectamine 3000 (Invitrogen) on the day 3 of differentiation, following the manufacturer's protocol. Eight hours after transfection, cells continued to use medium with 1.25% DMSO for another 2 days.

RNA extraction and real-time quantitative reverse transcription PCR (qRT-PCR)
Total RNA was extracted using the RNA-Quick Purification kit (YiShan Biotech, China). Reverse transcription was performed by PrimeScript™

Master Mix (TaKaRa, Japan) and followed with the SYBR Green Master Mix (TaKaRa, Japan). The following primers were used: MIF (Forward primer: AGAACCGCTCCTACAGCAAGCT, Reverse primer: GGAGTTGTTCCAGCCCACATTG), GAPDH (Forward primer: GGAGCGAGATCCCTCCAAAAT, Reverse primer: GGCTGTTGTCA-TACTTCTCATGG), CD11b (Forward primer: GGAACGC-CATTGTCTGCTTTCG, Reverse primer: ATGCTGAGGTCATCCTGGCAGA).

Western blot assay
Cells were lysed in RIPA lysis buffer (Beyotime, China) containing 1% protease and 2% phosphatase inhibitors (Thermo Fisher Scientific, USA). Proteins were separated by electrophoresis and transferred into poly-vinylidene fluoride (PVDF) membranes (Merck-Millipore, Germany) using a wet transfer system. After blocking with blocking solution (Beyotime, China), the membranes were incubated overnight with primary antibodies including AKT (Proteintech, 60203-2-Ig), Phospho-AKT (Proteintech, 80455-1-RR), ERK1/2 (Proteintech, 11257-1-AP), Phospho- ERK1/2 (CST, 4370 T), Vimentin (CST, 5741 T), E-cadherin (CST, 3195 T), N-cadherin (CST, 13116 T), β-Tubulin (CST, 2146S) and β-Actin (CST, 3700S) at 4 °C. Subsequently, secondary antibodies were utilized. Finally, the target proteins were detected by the enhanced chemiluminescence system.

Cell proliferation assay
AsPC-1, PANC-1, and CFPAC-1 cells were seeded in 96-well plates and treated with supernatants derived from either control or MIF-overexpressing dHL-60 cells, the MIF inhibitor 4-iodo-6-phenylpyrimidine (4-IPP, MedChemExpress, HY-110063), or vehicle. Cell viability was determined at 24-h intervals using the Cell Counting Kit-8 (Dojindo, Japan) according to the manufacturer's protocol.

EdU assay
In co-culture experiments, 24 mm transwell plates with a 0.4 µm pore polyester membrane insert (Corning, USA) were utilized. The dHL-60 cells were cultured in the upper chambers, while PDAC cells were cultured in the lower chambers. Following 2 days of co-culturing with control and MIF-overexpressed dHL-60 cells, EdU was added to the culture medium and PDAC cells were incubated for 2 h. The incorporation of EdU was detected using the BeyoClick™ EdU Cell Proliferation Kit with Alexa Fluor 488 (Beyotime, C0071S), following the manufacturer's instructions. The nuclei were counterstained with Hoechst 33342 and the cells were imaged using a fluorescence microscope.

Colony formation assay
PDAC cells were plated in 6-well plates (1000 cells/well) and treated with conditioned media from either control or MIF-overexpressing dHL-60 cells, the MIF inhibitor 4-IPP, or vehicle control. Following 1 week of incubation, colonies were fixed and stained with crystal violet.

Wound-healing assay
After 48 h of coculture with either control dHL-60 cells, MIF-overexpressing dHL-60 cells, 4-IPP, or vehicle, PDAC cells were seeded in Culture-Insert 2 Well (Ibidi, Germany) and cultured with serum-free DMEM. The area of each scratch was imaged by microscope at 0 and 24 h.

Transwell assay
After 48 h of coculture with either control dHL-60 cells, MIF-overexpressing dHL-60 cells, 4-IPP, or vehicle, PDAC cells were seeded into the upper chamber of transwell plates (8 µm pore size; Corning) with serum-free DMEM and incubated at 37 °C for 24 h. Migrated cells were stained with crystal violet and imaged by microscope.

Statistical analysis
All the data are presented as the means and standard deviations (SDs). Kaplan−Meier survival curves and log-rank tests were used to compare

Article

overall survival across different patient groups. Comparisons between two groups were performed with Student's *t* test. GraphPad Prism and R were used to perform the statistical analyses. Statistical significance is indicated as follows: *$p < 0.05$, **$p < 0.01$, and ***$p < 0.001$.

Data availability
The scRNA-seq data for PDAC patients were sourced from the Gene Expression Omnibus (GEO) database (https://www.ncbi.nlm.nih.gov/geo/), specifically, the GSE155698 and GSE205013 datasets. The TCGA-PAAD data were downloaded from UCSC Xena database (https://xena.ucsc.edu/). The original data are included in the article, which can also be obtained by contacting the corresponding authors.

Code availability
The code can be obtained by contacting the corresponding authors.

References
1. Siegel, R. L., Miller, K. D., Fuchs, H. E. & Jemal, A. Cancer statistics, 2021. *CA Cancer J. Clin.* **71**, 7–33 (2021).
2. Rahib, L. et al. Projecting cancer incidence and deaths to 2030: the unexpected burden of thyroid, liver, and pancreas cancers in the United States. *Cancer Res.* **74**, 2913–2921 (2014).
3. Mizrahi, J. D., Surana, R., Valle, J. W. & Shroff, R. T. Pancreatic cancer. *Lancet* **395**, 2008–2020 (2020).
4. Park, W., Chawla, A. & O'Reilly, E. M. Pancreatic cancer: a review. *Jama* **326**, 851–862 (2021).
5. Ho, W. J., Jaffee, E. M. & Zheng, L. The tumour microenvironment in pancreatic cancer - clinical challenges and opportunities. *Nat. Rev. Clin. Oncol.* **17**, 527–540 (2020).
6. Schizas, D. et al. Immunotherapy for pancreatic cancer: a 2020 update. *Cancer Treat. Rev.* **86**, 102016 (2020).
7. Hinshaw, D. C. & Shevde, L. A. The tumor microenvironment innately modulates cancer progression. *Cancer Res.* **79**, 4557–4566 (2019).
8. Jaillon, S. et al. Neutrophil diversity and plasticity in tumour progression and therapy. *Nat. Rev. Cancer* **20**, 485–503 (2020).
9. Hedrick, C. C. & Malanchi, I. Neutrophils in cancer: heterogeneous and multifaceted. *Nat. Rev. Immunol.* **22**, 173–187 (2022).
10. Németh, T., Sperandio, M. & Mócsai, A. Neutrophils as emerging therapeutic targets. *Nat. Rev. Drug Discov.* **19**, 253–275 (2020).
11. Stone, M. L. & Beatty, G. L. Cellular determinants and therapeutic implications of inflammation in pancreatic cancer. *Pharmacol. Ther.* **201**, 202–213 (2019).
12. Bianchi, A. et al. Cell-autonomous Cxcl1 sustains tolerogenic circuitries and stromal inflammation via neutrophil-derived TNF in pancreatic cancer. *Cancer Discov.* **13**, 1428–1453 (2023).
13. Bellomo, G. et al. Chemotherapy-induced infiltration of neutrophils promotes pancreatic cancer metastasis via Gas6/AXL signalling axis. *Gut* **71**, 2284–2299 (2022).
14. Han, J., DePinho, R. A. & Maitra, A. Single-cell RNA sequencing in pancreatic cancer. *Nat. Rev. Gastroenterol. Hepatol.* **18**, 451–452 (2021).
15. Cephas, A. T., Hwang, W. L., Maitra, A., Parnas, O. & DelGiorno, K. E. It is better to light a candle than to curse the darkness: single-cell transcriptomics sheds new light on pancreas biology and disease. *Gut* **72**, 1211–1219 (2023).
16. Bärthel, S., Falcomatà, C., Rad, R., Theis, F. J. & Saur, D. Single-cell profiling to explore pancreatic cancer heterogeneity, plasticity and response to therapy. *Nat. Cancer* **4**, 454–467 (2023).
17. Steele, N. G. et al. Multimodal mapping of the tumor and peripheral blood immune landscape in human pancreatic cancer. *Nat. Cancer* **1**, 1097–1112 (2020).
18. Chen, K. et al. Single-cell RNA-seq reveals dynamic change in tumor microenvironment during pancreatic ductal adenocarcinoma malignant progression. *EBioMedicine* **66**, 103315 (2021).
19. Xue, R. et al. Liver tumour immune microenvironment subtypes and neutrophil heterogeneity. *Nature* **612**, 141–147 (2022).
20. Salcher, S. et al. High-resolution single-cell atlas reveals diversity and plasticity of tissue-resident neutrophils in non-small cell lung cancer. *Cancer Cell* **40**, 1503–1520.e1508 (2022).
21. Hu, S. et al. TDO2+ myofibroblasts mediate immune suppression in malignant transformation of squamous cell carcinoma. *J. Clin. Investig.* **132**, e157649 (2022).
22. Wu, Y. et al. Neutrophil profiling illuminates anti-tumor antigen-presenting potency. *Cell* **187**, 1422–1439.e1424 (2024).
23. Wang, L. et al. Single-cell RNA-seq analysis reveals BHLHE40-driven pro-tumour neutrophils with hyperactivated glycolysis in pancreatic tumour microenvironment. *Gut* **72**, 958–971 (2023).
24. Mahiddine, K. et al. Relief of tumor hypoxia unleashes the tumoricidal potential of neutrophils. *J. Clin. Investig.* **130**, 389–403 (2020).
25. Adrover, J. M., McDowell, S. A. C., He, X. Y., Quail, D. F. & Egeblad, M. NETworking with cancer: the bidirectional interplay between cancer and neutrophil extracellular traps. *Cancer Cell* **41**, 505–526 (2023).
26. Kim, R. et al. Ferroptosis of tumour neutrophils causes immune suppression in cancer. *Nature* **612**, 338–346 (2022).
27. Sumaiya, K., Langford, D., Natarajaseenivasan, K. & Shanmughapriya, S. Macrophage migration inhibitory factor (MIF): a multifaceted cytokine regulated by genetic and physiological strategies. *Pharmacol. Ther.* **233**, 108024 (2022).
28. Funamizu, N. et al. Macrophage migration inhibitory factor induces epithelial to mesenchymal transition, enhances tumor aggressiveness and predicts clinical outcome in resected pancreatic ductal adenocarcinoma. *Int. J. Cancer* **132**, 785–794 (2013).
29. Shaul, M. E. & Fridlender, Z. G. Tumour-associated neutrophils in patients with cancer. *Nat. Rev. Clin. Oncol.* **16**, 601–620 (2019).
30. Hegde, S., Leader, A. M. & Merad, M. MDSC: markers, development, states, and unaddressed complexity. *Immunity* **54**, 875–884 (2021).
31. Ng, M. S. F. et al. Deterministic reprogramming of neutrophils within tumors. *Science* **383**, eadf6493 (2024).
32. Yin, W. et al. CCRL2 promotes antitumor T-cell immunity via amplifying TLR4-mediated immunostimulatory macrophage activation. *Proceedings of the National Academy of Sciences of the United States of America* **118** (2021).
33. Evrard, M. et al. Developmental analysis of bone marrow neutrophils reveals populations specialized in expansion, trafficking, and effector functions. *Immunity* **48**, 364–379.e368 (2018).
34. Martin, C. et al. Chemokines acting via CXCR2 and CXCR4 control the release of neutrophils from the bone marrow and their return following senescence. *Immunity* **19**, 583–593 (2003).
35. Steele, C. W. et al. CXCR2 inhibition profoundly suppresses metastases and augments immunotherapy in pancreatic ductal adenocarcinoma. *Cancer Cell* **29**, 832–845 (2016).
36. Teijeira, Á et al. CXCR1 and CXCR2 chemokine receptor agonists produced by tumors induce neutrophil extracellular traps that interfere with immune cytotoxicity. *Immunity* **52**, 856–871.e858 (2020).
37. Yang, J. et al. Loss of CXCR4 in myeloid cells enhances antitumor immunity and reduces melanoma growth through NK cell and FASL mechanisms. *Cancer Immunol. Res.* **6**, 1186–1198 (2018).
38. Penticuff, J. C., Woolbright, B. L., Sielecki, T. M., Weir, S. J. & Taylor, J. A. 3rd MIF family proteins in genitourinary cancer: tumorigenic roles and therapeutic potential. *Nat. Rev. Urol.* **16**, 318–328 (2019).
39. Thiele, M., Donnelly, S. C. & Mitchell, R. A. OxMIF: a druggable isoform of macrophage migration inhibitory factor in cancer and inflammatory diseases. *J. Immunother. Cancer* **10**, e005475 (2022).
40. Wen, Y. et al. Targeting macrophage migration inhibitory factor in acute pancreatitis and pancreatic cancer. *Front. Pharmacol.* **12**, 638950 (2021).

41. Costa-Silva, B. et al. Pancreatic cancer exosomes initiate pre-metastatic niche formation in the liver. *Nat. Cell Biol.* **17**, 816–826 (2015).

42. Yang, S. et al. A novel MIF signaling pathway drives the malignant character of pancreatic cancer by targeting NR3C2. *Cancer Res.* **76**, 3838–3850 (2016).

43. Jia, X. et al. The tautomerase activity of tumor exosomal MIF promotes pancreatic cancer progression by modulating MDSC differentiation. *Cancer Immunol. Res.* **12**, 72–90 (2024).

44. Collins, S. J., Ruscetti, F. W., Gallagher, R. E. & Gallo, R. C. Terminal differentiation of human promyelocytic leukemia cells induced by dimethyl sulfoxide and other polar compounds. *Proc. Natl. Acad. Sci. USA* **75**, 2458–2462 (1978).

45. Zhang, J. F. et al. CD74 promotes perineural invasion of cancer cells and mediates neuroplasticity via the AKT/EGR-1/GDNF axis in pancreatic ductal adenocarcinoma. *Cancer Lett.* **508**, 47–58 (2021).

46. Wang, D. et al. Upregulation of macrophage migration inhibitory factor promotes tumor metastasis and correlates with poor prognosis of pancreatic ductal adenocarcinoma. *Oncol. Rep.* **40**, 2628–2636 (2018).

47. Lue, H. et al. Macrophage migration inhibitory factor (MIF) promotes cell survival by activation of the Akt pathway and role for CSN5/JAB1 in the control of autocrine MIF activity. *Oncogene* **26**, 5046–5059 (2007).

48. Zhu, G. Q. et al. CD36(+) cancer-associated fibroblasts provide immunosuppressive microenvironment for hepatocellular carcinoma via secretion of macrophage migration inhibitory factor. *Cell Discov.* **9**, 25 (2023).

Author contributions

Yan Zeng and Linjuan Zeng conceived the original idea and designed the experiments. Yan Zeng and Jiaping Yu wrote the code and performed the computational analyses. Juan Zhuang performed the experiments and analyzed the data. Xinyue Liang and Yaning Li contributed to the interpretation of the results. Yutong Chen drafted the manuscript. Shili Chen and Wenzheng Pang revised and validated the manuscript. All the authors reviewed the manuscript.

Competing interests

The authors declare no competing interests.

Additional information

Supplementary information The online version contains supplementary material available at https://doi.org/10.1038/s41698-025-01085-3.

Correspondence and requests for materials should be addressed to Shili Chen, Wenzheng Pang or Linjuan Zeng.

Reprints and permissions information is available at http://www.nature.com/reprints

Publisher's note Springer Nature remains neutral with regard to jurisdictional claims in published maps and institutional affiliations.